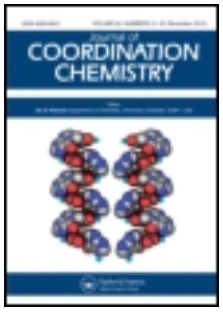

Journal of Coordination Chemistry
Publication details, including instructions for authors and subscription information:
http://www.tandfonline.com/loi/gcoo20

Dinuclear rare-earth picrate complexes based on a multidentate amide ligand: syntheses, crystal structures, and luminescence properties

Wei Wang [a], Yong Huang [a], Tong Li [a], Guang-Nong Lu [a], Ying Yang [a], Ning Tang [a] & Hai-Bin Song [b]

[a] Key Laboratory of Nonferrous Metals Chemistry and Resources Utilization of Gansu Province, College of Chemistry and Chemical Engineering, Lanzhou University, Lanzhou 730000, Gansu, P.R. China

[b] The State Key Laboratory of Elemento-Organic Chemistry, Nankai University, Tianjin 300071, P.R. China

Accepted author version posted online: 18 Sep 2012.Published online: 03 Oct 2012.

To cite this article: Wei Wang, Yong Huang, Tong Li, Guang-Nong Lu, Ying Yang, Ning Tang & Hai-Bin Song (2012) Dinuclear rare-earth picrate complexes based on a multidentate amide ligand: syntheses, crystal structures, and luminescence properties, Journal of Coordination Chemistry, 65:22, 4041-4053, DOI: 10.1080/00958972.2012.731503

To link to this article: http://dx.doi.org/10.1080/00958972.2012.731503

Journal of Coordination Chemistry
Vol. 65, No. 22, 20 November 2012, 4041–4053

Dinuclear rare-earth picrate complexes based on a multidentate amide ligand: syntheses, crystal structures, and luminescence properties

WEI WANG†, YONG HUANG*†, TONG LI†, GUANG-NONG LU†, YING YANG†, NING TANG*† and HAI-BIN SONG‡

†Key Laboratory of Nonferrous Metals Chemistry and Resources Utilization of Gansu Province, College of Chemistry and Chemical Engineering, Lanzhou University, Lanzhou 730000, Gansu, P.R. China
‡The State Key Laboratory of Elemento-Organic Chemistry, Nankai University, Tianjin 300071, P.R. China

(*Received 1 January 2012; in final form 27 August 2012*)

A new amide-based multidentate ligand, *N*,*N*′-1,2-ethanediyl-bis{2-[(*N*,*N*-diethylcarbamoyl)-methoxy]benzamide} (L) reacts with $M(Pic)_3 \cdot 6H_2O$ to give rare-earth picrate complexes $[M_2L_2(Pic)_4(H_2O)_2](Pic)_2$ (M = La (**1**), Nd (**2**), Eu (**3**), Gd (**4**), Tb (**5**), Dy (**6**), Yb (**7**), Y (**8**)). X-ray single-crystal diffraction analyses indicate that dinuclear complexes $\mathbf{3} \cdot 2C_4H_8O_2$, $\mathbf{6} \cdot 2C_4H_8O_2$, and $\mathbf{8} \cdot 2CH_3CN$ are isomorphous. Each metal is nine-coordinate by four oxygen atoms of two ligands, four oxygen atoms of two bidentate picrates, and one water molecule with a distorted monocapped square antiprism. With hydrogen bonds between the free picrate anions and the coordination cations the complexes exhibit 2-D layers. The luminescent properties of **3** $[Eu_2L_2(Pic)_4(H_2O)_2](Pic)_2$ are described and factors that influence luminescent intensities are also discussed.

Keywords: Rare-earth complex; Dinuclear complex; Crystal structure; Luminescence properties

1. Introduction

Rare-earth complexes attract attention due to their unique luminescence properties (long, millisecond-order lifetime, large Stokes' shift and narrow emission bands) [1] and their important applications as labels and sensors in materials and probes in biological systems [2–4]. However, rare-earth ions have poor direct light absorption as a result of the parity-forbidden 4f–4f transitions [5]. As a result, luminescence intensity of rare-earth complexes is strongly dependent on the efficiency of ligand absorption in the UV region, the efficiency of ligand to metal energy transfer, and the efficiency of rare-earth luminescence, the well-known "antenna effect" [6]. Rare-earth ions adopt a range of coordination numbers between 6 and 12 to form flexible coordination geometries; the photoluminescence intensity of rare-earth complexes shows hypersensitivity to

*Corresponding authors. Email: huangyong@lzu.edu.cn; tangn@lzu.edu.cn

ISSN 0095-8972 print/ISSN 1029-0389 online
http://dx.doi.org/10.1080/00958972.2012.731503

coordination environment and molecular structures [1, 7]. Therefore, to synthesize an ideal multidentate organic ligand which coordinates with rare-earth ions, improving the absorption and forming new structures are a challenge. Bifunctional ligands such as macrocycles [8, 9], podand-type ligands [10], carboxylic acid derivatives [11, 12], and β-diketone derivatives [13, 14] have been synthesized and used as antennas to improve the poor absorption of rare-earth ions. High denticity acyclic polyethers encapsulate the metal ion and protect it from solvent interactions, offering many advantages in extraction and analysis of rare-earth ions [15]. Nevertheless, to achieve good luminescence and optimal binding, it is also important to get the right balance between flexibility and rigidity [16].

Recently, we have designed a series of functional acyclic polyethers having both selective ability to coordinate rare-earth ions and enhanced luminescence of rare-earth complexes, by selecting amide as conjugate groups and providing a protective environment for the rare-earth ion. Also, picrates as the bulky counter anions have been used to influence structures of rare-earth complexes and the triplet state energy level of the ligands [17, 18]. As part of our systematic studies, a new, doubly functionalized multidentate ligand, *N*,*N*′-1,2-ethanediyl-bis{2-[(*N*,*N*-diethylcarbamoyl)-methoxy]benzamide} (L) and the corresponding rare-earth picrate complexes (scheme 1) have been prepared. The coordination and luminescence properties of rare-earth picrate complexes show that europium complex emits the intrinsic spectrum of Eu(III) ions under excitation of ultraviolet light, and the solvents affect the luminescence.

2. Experimental

2.1. *Materials and methods*

Rare-earth picrates $M(Pic)_3 \cdot 6H_2O$ [19], *N*,*N*′-1,2-ethanediyl-bis(2-hydroxybenzamide) [20] and *N*,*N*-diethyl-2-chloroacetamide [21] were prepared according to literature methods. Other reagents purchased commercially were of A.R. grade and used without purification. Carbon, hydrogen, and nitrogen analyses were obtained using an Elementar Vario EL elemental analyzer. The rare-earth ions were determined by EDTA titration using xylenol orange as indicator. Conductivity measurements were carried out in 10^{-3} mol $\cdot$ cm^{-3} solutions at 25°C using a DDS-307 conductivity meter. IR spectra from 4000 to 400 cm^{-1} were measured using KBr pellets on a Nicolet Nexus 670 FTIR spectrometer. ^{1}H NMR spectra were recorded on a Varian Mercury 400 BB

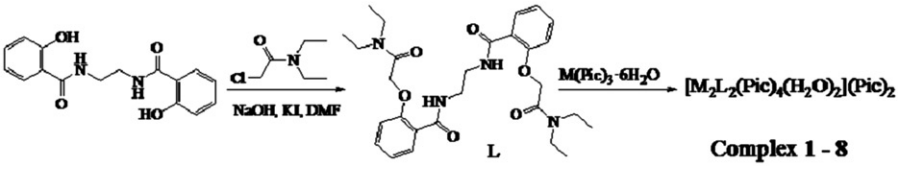

Scheme 1. The synthetic route of L and rare-earth picrate complexes **1–8**.

using $CDCl_3$ as solvent and TMS as internal standard. The excitation and luminescence spectra were performed on a Hitachi F-4500 spectrophotometer.

2.2. *Synthesis of the ligand L*

N,*N*′-1,2-ethanediyl-bis(2-hydroxybenzamide) (2.40 g, 8.0 mmol) and sodium hydroxide (0.64 g, 16.0 mmol) in DMF (100 cm^3) were heated to 80°C and stirred for 0.5 h. Then a solution of *N*,*N*-diethyl-2-chloroacetamide (2.63 g, 17.6 mmol) and KI (catalytic amount) in DMF (50 cm^3) was added dropwise. The reaction mixture was stirred at 80°C for an additional 15 h and then concentrated in vacuum. The resultant solid was recrystallized with ethanol twice to give 2.95 g of colorless prism crystals. Yield: 70%; m.p. 168–171°C. ^{1}H NMR ($CDCl_3$, ppm): δ 9.55 (s, 2H, –CO–N*H*–), 6.91–8.12 (m, 8H, Ar–*H*), 4.90 (s, 4H, CH_2–O), 3.83 (m, 4H, CH_2–CH_2–N), 3.27–3.34 (q, 8H, CH_3–CH_2–N), 1.04–1.20 (d and t, 12H, –CH_3). IR (KBr, cm^{-1}): 3305(s, ν(N–H)), 3075(m, Ph–H), 2969(m, C–H), 2927(m, C–H), 1659(s, C=O), 1627(s, C=O), 1599(m, C=C), 1540(m), 1487(m), 1248(m, Ar–O–C), 1107(m), 1068(m), 871(m), 758(m). Anal. Calcd (%) for $C_{28}H_{38}N_4O_6$: C, 63.86; H, 7.27; N, 10.64; O, 18.23. Found (%): C, 63.83; H, 7.20; N, 10.72; O, 18.25.

2.3. *Syntheses of 1–8*

A solution of 0.2 mmol rare-earth picrates $M(Pic)_3 \cdot 6H_2O$ (M = La, Nd, Eu, Gd, Tb, Dy, Yb, Y) in 10 cm^3 of ethyl acetate was added to a solution of 0.2 mmol L in 10 cm^3 of chloroform. The mixture was stirred for 6 h at room temperature. The precipitated yellow solid was separated from the solution by suction filtration, purified by washing several times with ethyl acetate and chloroform, and then dried for 24 h in a vacuum over P_4O_{10} at room temperature (yield 80%). Elemental analyses are in good agreement with stoichiometries of all complexes.

2.3.1. $[La_2L_2(Pic)_4(H_2O)_2](Pic)_2$ (1). Anal. Calcd for $C_{92}H_{92}La_2N_{26}O_{56}$ (%): C, 40.39; H, 3.39; N, 13.31; O, 32.75; La, 10.16. Found (%): C, 40.46; H, 3.67; N, 13.12; O, 32.85; La, 10.30. IR (KBr, cm^{-1}): 3325(m, ν(O–H, N–H)); 3090(m, Ph–H), 2972(m, C–H), 2930(m, C–H), 1626(s, ν(C=O)), 1613(s, ν(C=O)); 1575(s, ν_{as}(–NO_2)), 1543(s, ν_{as}(–NO_2)); 1488(m), 1360(s, ν_s(–NO_2)), 1331(s, ν_s(–NO_2)); 1274(s, ν(C–O)); 1245(m, ν(Ar–O–C)), 1221(m, ν(Ar–O–C)), 1077(m), 1046(m), 845(m), 753(m), 710(m).

2.3.2. $[Nd_2L_2(Pic)_4(H_2O)_2](Pic)_2$ (2). Anal. Calcd for $C_{92}H_{92}N_{26}Nd_2O_{56}$ (%): C, 40.24; H, 3.38; N, 13.26; O, 32.62; Nd, 10.50. Found (%): C, 40.13; H, 3.29; N, 13.43; O, 33.04; Nd, 10.11. IR (KBr, cm^{-1}): 3320(m, ν(O–H, N–H)); 3094(m, Ph–H), 2977(m, C–H), 2935(m, C–H), 1623(m, ν(C=O)), 1614(s, ν(C=O)); 1574(s, ν_{as}(–NO_2)), 1541(s, ν_{as}(–NO_2)); 1490(m), 1360(s, ν_s(–NO_2)), 1330(s, ν_s(–NO_2)); 1272(s, ν(C–O)); 1246(m, ν(Ar–O–C)), 1220(m, ν(Ar–O–C)), 1080(m), 1048(m), 845(m), 755(m), 710(m).

2.3.3. $[Eu_2L_2(Pic)_4(H_2O)_2](Pic)_2$ (3). Anal. Calcd for $C_{92}H_{92}Eu_2N_{26}O_{56}$ (%): C, 40.01; H, 3.36; N, 13.19; O, 32.44; Eu, 11.00. Found (%): C, 39.96; H, 3.37; N,

13.26; O, 32.50; Eu, 10.91. IR (KBr, cm^{-1}): 3328(m, ν(O–H, N–H)); 3094(m, Ph–H), 2977(m, C–H), 2935(m, C–H), 1628(m, ν(C=O)), 1614(s, ν(C=O)); 1574(s, ν_{as}(–NO_2)), 1540(s, ν_{as}(–NO_2)); 1490(m), 1361(s, ν_s(–NO_2)), 1330(s, ν_s(–NO_2)); 1272(s, ν(C–O)); 1247(m, ν(Ar–O–C)), 1220(m, ν(Ar–O–C)), 1080(m), 1048(m), 847(m), 755(m), 710(m).

2.3.4. $[Gd_2L_2(Pic)_4(H_2O)_2](Pic)_2$ (4). Anal. Calcd for $C_{92}H_{92}Gd_2N_{26}O_{56}$ (%): C, 39.86; H, 3.34; N, 13.14; O, 32.32; Gd, 11.34. Found (%): C, 39.65; H, 3.67; N, 13.08; O, 32.58; Gd, 11.02. IR (KBr, cm^{-1}): 3317(m, ν(O–H, N–H)); 3088(m, Ph–H), 2970(m, C–H), 2930(m, C–H), 1626(s, ν(C=O)), 1614(s, ν(C=O)); 1574(s, ν_{as}(–NO_2)), 1542(s, ν_{as}(–NO_2)); 1488(m), 1360(s, ν_s(–NO_2)), 1330(s, ν_s(–NO_2)); 1272(s, ν(C–O)); 1248(m, ν(Ar–O–C)), 1220(m, ν(Ar–O–C)), 1078(m), 1047(m), 842(m), 754(m), 710(m).

2.3.5. $[Tb_2L_2(Pic)_4(H_2O)_2](Pic)_2$ (5). Anal. Calcd for $C_{92}H_{92}N_{26}O_{56}Tb_2$ (%): C, 39.81; H, 3.34; N, 13.12; O, 32.28; Tb, 11.45%. Found (%): C, 39.54; H, 3.23; N, 12.95; O, 32.90; Tb, 11.38%. IR (KBr, cm^{-1}): 3318(m, ν(O–H, N–H)); 3087(m, Ph–H), 2970(m, C–H), 2928(m, C–H), 1627(s, ν(C=O)), 1614(s, ν(C=O)); 1576(s, ν_{as}(–NO_2)), 1542(s, ν_{as}(–NO_2)); 1488(m), 1361(s, ν_s(–NO_2)), 1330(s, ν_s(–NO_2)); 1271(s, ν(C–O)); 1248(m, ν(Ar–O–C)), 1221(m, ν(Ar–O–C)), 1076(m), 1045(m), 846(m), 755(m), 711(m).

2.3.6. $[Dy_2L_2(Pic)_4(H_2O)_2](Pic)_2$ (6). Anal. Calcd for $C_{92}H_{92}Dy_2N_{26}O_{56}$ (%): C, 39.71; H, 3.33; N, 13.09; O, 32.19; Dy, 11.68. Found (%): C, 39.80; H, 3.17; N, 13.01; O, 32.19; Dy, 11.83. IR (KBr, cm^{-1}): 3307(m, ν(O–H, N–H)); 3088(m, Ph–H), 2970(m, C–H), 2928(m, C–H), 1626(s, ν(C=O)), 1615(s, ν(C=O)); 1573(s, ν_{as}(–NO_2)), 1545(s, ν_{as}(–NO_2)); 1487(m), 1360(s, ν_s(–NO_2)), 1330(s, ν_s(–NO_2)); 1274(s, ν(C–O)); 1248(m, ν(Ar–O–C)), 1222(m, ν(Ar–O–C)), 1078(m), 1046(m), 842(m), 752(m), 710(m).

2.3.7. $[Yb_2L_2(Pic)_4(H_2O)_2](Pic)_2$ (7). Anal. Calcd for $C_{92}H_{92}N_{26}O_{56}Yb_2$ (%): C, 39.41; H, 3.31; N, 12.99; O, 31.95; Yb, 12.34. Found (%): C, 39.45; H, 3.58; N, 13.17; O, 32.31; Yb, 12.49. IR (KBr, cm^{-1}): 3312(m, ν(O–H, N–H)); 3091(m, Ph–H), 2973(m, C–H), 2930(m, C–H), 1625(s, ν(C=O)), 1614(s, ν(C=O)); 1573(s, ν_{as}(–NO_2)), 1542(s, ν_{as}(–NO_2)); 1487(m), 1361(s, ν_s(–NO_2)), 1332(s, ν_s(–NO_2)); 1272(s, ν(C–O)); 1248(m, ν(Ar–O–C)), 1221(m, ν(Ar–O–C)), 1077(m), 1050(m), 845(m), 758(m), 709(m).

2.3.8. $[Y_2L_2(Pic)_4(H_2O)_2](Pic)_2$ (8). Anal. Calcd for $C_{92}H_{92}N_{26}O_{56}Y_2$ (%): C, 41.93; H, 3.52; N, 13.82; O, 33.98; Y, 6.75. Found (%): C, 41.67; H, 3.58; N, 13.68; O, 34.58; Y, 6.49. IR (KBr, cm^{-1}): 3305(m, ν(O–H, N–H)); 3094(m, Ph–H), 2975(m, C–H), 2932(m, C–H), 1627(s, ν(C=O)), 1615(s, ν(C=O)); 1573(s, ν_{as}(–NO_2)), 1543(s, ν_{as}(–NO_2)); 1488(m), 1361(s, ν_s(–NO_2)), 1331(s, ν_s(–NO_2)); 1273(s, ν(C–O)); 1248(m, ν(Ar–O–C)), 1220(m, ν(Ar–O–C)), 1078(m), 1051(m), 844(m), 759(m), 708(m).

2.4. *Single-crystal structure determination*

Determinations of the unit cell and crystallographic data collection were performed with graphite-monochromated Mo-Kα radiation ($\lambda = 0.71073$ Å) at 293(2)/113(2) K on a BRUKER SMART 1000 diffractometer equipped with a CCD camera. The ω–φ scan

technique was employed. SAINT [22] was used for integration of the diffraction profiles. The structures were solved primarily by direct methods and secondly by Fourier difference techniques and refined by full-matrix least-squares using the SHELXS program of the SHELXTL package [23]. Metals in each complex were located from the *E*-maps, and other non-hydrogen atoms were located in successive difference Fourier syntheses and refined with anisotropic thermal parameters on F^2. Hydrogen atoms were set in calculated positions and refined as riding with a common fixed isotropic thermal parameter (hydrogen atoms of coordinated water were located using the difference Fourier method).

3. Results and discussion

3.1. *Syntheses of complexes*

The synthetic routes for the multidentate amide L and **1**–**8** are shown in scheme 1. All the picrate complexes are air stable, yellow powders, and soluble in DMSO, DMF, methanol, ethanol, acetone, acetonitrile, and ethyl acetate, slightly soluble in diethyl ether and chloroform, but insoluble in benzene and water. All the picrate complexes are characterized by elemental and spectral analyses. The analytical data for the complexes indicate that all conform to a 2 : 2 metal-to-ligand stoichiometry, which is in accord with the results of crystal structure determinations. The molar conductance values of the complexes in DMF (106–143 $S\,cm^2\,mol^{-1}$) indicate the presence of a 1 : 2 type electrolyte [24], implying that two picrates are counter anions outside the coordination sphere.

3.2. *Descriptions of crystal structures*

Crystals of $\mathbf{3}\cdot 2C_4H_8O_2$, $\mathbf{6}\cdot 2C_4H_8O_2$, and $\mathbf{8}\cdot 2CH_3CN$ were grown by slow evaporation from methanol and ethyl acetate (or acetonitrile) mixed solution at room temperature over a period of several weeks. The crystallographic data and structure determination parameters are summarized in table 1 and selected bond lengths and angles are listed in table 2. The structure analyses show that the dinuclear complexes are isomorphous. Each complex has one $[M_2L_2(Pic)_4(H_2O)_2]^{2+}$ (figure 1), two free picrates as counter anions, and two solvents (ethyl acetate or acetonitrile) linked by van der Waals' forces. The ligands are tetradentate and coordinate to one metal ion by two carbonyl and one phenoxy oxygen atoms and to another metal ion by another carbonyl. The three complexes show nine coordination with oxygen donors, four from two L, four from two bidentate picrates, and the last from one water molecule. The coordination polyhedron is a distorted monocapped square antiprism in which O_6, O_4, O_8, O_{3A} and O_7, O_9, O_{15}, O_{16} define, respectively, the upper and lower tetragonal faces of the antiprism, the former being capped by O_5 (figure 2, complex $\mathbf{3}\cdot 2C_4H_8O_2$ for an example).

With smaller central metal the average distances between the metal ions and the coordinated oxygen become slightly shorter (Eu, 2.462 Å; Dy, 2.422 Å; Y, 2.415 Å). The M–O (C=O) distances [mean to Eu 2.313(2)–2.366(2) Å, to Dy 2.280(2)–2.327(3) Å and to Y 2.2667(17)–2.314(3) Å] are much shorter than the M–O (C–O–C) [mean to Eu 2.811(2) Å, to Dy 2.798(2) Å and to Y 2.7759(19) Å] distances, suggesting that the M–O (C=O) bond is stronger than the M–O (C–O–C). The M–O distances agree with those

Table 1. Crystallographic data for **3**·2$CH_3COOC_2H_5$, **6**·2$CH_3COOC_2H_5$, and **8**·2CH_3CN.

Parameters	**3**·2$CH_3COOC_2H_5$	**6**·2$CH_3COOC_2H_5$	**8**·2CH_3CN
Crystal shape	Block	Block	Block
Color	Yellow	Yellow	Yellow
Size (mm^3)	$0.24 \times 0.20 \times 0.18$	$0.14 \times 0.16 \times 0.10$	$0.32 \times 0.12 \times 0.10$
Formula	$C_{100}H_{108}Eu_2N_{26}O_{60}$	$C_{100}H_{108}Dy_2N_{26}O_{60}$	$C_{96}H_{98}N_{28}O_{56}Y_2$
Formula weight	2938.04	2959.12	2717.84
Crystal system	Triclinic	Triclinic	Triclinic
Space group	*P*-1	*P*-1	*P*-1
Unit cell dimensions (Å, °)			
a	12.9244(13)	12.758(3)	12.307(3)
b	12.9846(13)	12.845(3)	12.575(2)
c	20.779(2)	20.548(5)	20.451(4)
α	93.285(2)	93.136(3)	93.6070(10)
β	107.671(2)	107.751(2)	106.960(2)
γ	109.814(2)	109.805(2)	108.327(2)
Volume ($Å^3$), *Z*	3075.5(5), 1	2970.1(12), 1	2832.0(9), 1
Calculated density (Mg m^{-3})	1.586	1.654	1.594
Absorption coefficient (mm^{-1})	1.121	1.363	1.135
F(000)	1496	1502	1396
2θ range for data collection (°)	4.7–52.64	3.4–55.8	3.46–55.76
Index ranges	$-13 \le h \le 15$; $-15 \le k \le 14$; $-24 \le l \le 17$	$-14 \le h \le 15$; $-14 \le k \le 15$; $-24 \le l \le 18$	$-15 \le h \le 16$; $-15 \le k \le 16$; $-26 \le l \le 21$
Measured reflections	15,769	21,691	25,424
Unique reflections	10,780	10,419	13,277
Reflection used [$I > 2\sigma(I)$]	9119	9290	9617
Temperature (K)	293(2)	113(2)	113(2)
R_{int}	0.0235	0.0451	0.0414
R_1	0.0335	0.0368	0.0519
$wR_2[I > 2\sigma(I)]$	0.0736	0.0758	0.1075
Goodness-of-fit on F^2	1.035	1.041	1.016

found in similar complexes and the changes are related to balance between flexibility and rigidity of the ligand containing different functional groups. Complex $\mathbf{3} \cdot 2C_4H_8O_2$, for example, has average Eu–O (C=O) bond length slightly shorter than that of $[EuL]^+$ (2.369 Å, L = 3,3,7,7-tetra[*N*-ethyl-*N*-phenyl(acetamide)-2oxymethyl]-5-oxanonane) [25] and $[Eu(L)_2(H_2O)_2(CF_3SO_3)]^{3+}$ (2.386(3)–2.463(3) Å, L = *N,N,N′,N′*-tetraisopropylpyridine-2,6-dicarboxamide) [26], but Eu–O (C–O–C) bond length is much longer than that of $[EuL]^+$ (2.486 Å) [25] mentioned above.

In each coordination cation, there exist intramolecular face-to-face $\pi \cdots \pi$ stacking interactions between phenyl rings of two ligands, as shown in figure 3. In **3**, the dihedral angle between planes is 8.00° with a centroid distance of 3.963 Å, while in **6** the dihedral angle is 7.55° with a centroid distance of 3.918 Å, and in **8** the dihedral angle is 9.42° with a centroid distance of 3.885 Å. The amides form intramolecular hydrogen bonds with both the carbonyl [N(2)–H(2)···O1] and phenoxy [N(2)–H(2)···O(2)]. Coordinated H_2O forms hydrogen bonds with the carbonyl [O(7)–H(7A)···O(1)] (figure 3 and table 3, $\mathbf{3} \cdot 2C_4H_8O_2$ for an example). Eu(1)···Eu(1A), Dy(1)···Dy(1A), Y(1)···Y(1A) separations of 8.009 Å, 8.321 Å, and 8.347 Å, respectively, are also in agreement with those of dinuclear complexes which have special properties for efficient energy conversion and transfer [7, 27, 28].

Table 2. Selected bond distances (Å) and angles (°) for **3**, **6**, and **8**.

Complex **3**·2$CH_3COOC_2H_5$			
Bond lengths			
Eu(1)–O(4)	2.313(3)	Eu(1)–O(3A)	2.334(3)
Eu(1)–O(6)	2.365(2)	Eu(1)–O(15)	2.387(3)
Eu(1)–O(9)	2.576(3)	Eu(1)–O(16)	2.590(3)
Eu(1)–O(5)	2.811(2)	Eu(1)–O(7)	2.447(2)
Eu(1)–O(8)	2.337(3)	Eu(1)–Eu(1A)	8.009
Bond angles			
O(4)–Eu(1)–O(3A)	77.55(9)	O(8)–Eu(1)–O(3A)	80.05(9)
O(5)–Eu(1)–O(8)	75.38(8)	O(8)–Eu(1)–O(6)	75.40(9)
O(4)–Eu(1)–O(7)	80.63(8)	O(3A)–Eu(1)–O(7)	83.05(8)
O(3A)–Eu(1)–O(9)	76.76(9)	O(15)–Eu(1)–O(7)	82.35(9)
O(15)–Eu(1)–O(9)	67.79(8)	O(8)–Eu(1)–O(9)	65.75(8)
O(15)–Eu(1)–O(16)	65.20(8)	O(9)–Eu(1)–O(7)	69.06(8)
O(4)–Eu(1)–O(5)	61.82(7)	O(16)–Eu(1)–O(7)	68.13(8)
O(6)–Eu(1)–O(5)	59.00(8)	O(3A)–Eu(1)–O(5)	76.46(8)
Complex **6**·2$CH_3COOC_2H_5$			
Bond lengths			
Dy(1)–O(2)	2.280(3)	Dy(1)–O(1A)	2.288(2)
Dy(1)–O(6)	2.327(3)	Dy(1)–O(14)	2.348(2)
Dy(1)–O(8)	2.531(3)	Dy(1)–O(15)	2.539(2)
Dy(1)–O(5)	2.798(2)	Dy(1)–O(28)	2.382(3)
Dy(1)–O(7)	2.301(2)	Dy(1)–Dy(1A)	8.321
Bond angles			
O(2)–Dy(1)–O(1A)	78.24(8)	O(7)–Dy(1)–O(1A)	79.90(9)
O(5)–Dy(1)–O(7)	74.20(8)	O(7)–Dy(1)–O(6)	74.45(9)
O(2)–Dy(1)–O(28)	80.57(9)	O(1A)–Dy(1)–O(28)	82.93(9)
O(1A)–Dy(1)–O(8)	75.74(8)	O(14)–Dy(1)–O(28)	83.20(9)
O(14)–Dy(1)–O(8)	67.58(8)	O(7)–Dy(1)–O(8)	66.65(8)
O(15)–Dy(1)–O(14)	66.39(8)	O(8)–Dy(1)–O(28)	68.98(9)
O(2)–Dy(1)–O(5)	62.05(8)	O(15)–Dy(1)–O(28)	67.87(9)
O(6)–Dy(1)–O(5)	59.36(7)	O(1A)–Dy(1)–O(5)	75.90(8)
Complex **8**·2CH_3CN			
Bond lengths			
Y(1)–O(2)	2.2667(17)	Y(1)–O(1A)	2.3059(18)
Y(1)–O(6)	2.314(2)	Y(1)–O(14)	2.3503(18)
Y(1)–O(8)	2.4862(19)	Y(1)–O(15)	2.5375(19)
Y(1)–O(5)	2.7759(19)	Y(1)–O(28)	2.384(2)
Y(1)–O(7)	2.3101(19)	Y(1)–Y(1A)	8.347
Bond angles			
O(2)–Y(1)–O(1A)	77.34(6)	O(7)–Y(1)–O(1A)	79.04(7)
O(5)–Y(1)–O(7)	72.96(6)	O(7)–Y(1)–O(6)	73.18(7)
O(2)–Y(1)–O(28)	80.29(7)	O(1A)–Y(1)–O(28)	84.91(7)
O(1A)–Y(1)–O(8)	76.84(6)	O(14)–Y(1)–O(28)	82.02(7)
O(14)–Y(1)–O(8)	68.61(6)	O(7)–Y(1)–O(8)	66.90(7)
O(15)–Y(1)–O(14)	66.39(6)	O(8)–Y(1)–O(28)	70.20(7)
O(2)–Y(1)–O(5)	62.35(6)	O(15)–Y(1)–O(28)	67.93(7)
O(6)–Y(1)–O(5)	59.67(6)	O(1A)–Y(1)–O(5)	75.30(6)

The packing diagram of **3** · $2C_4H_8O_2$, **6** · $2C_4H_8O_2$, and **8** · 2CH_3CN exhibit a 2-D supramolecular architecture arising from C–H···O and O–H···O hydrogen bonds, as shown in figure 4. Taking **3** as an example (table 3), the C–H···O interactions can be depicted by C···O distances and the C–H···O angle θ [29, 30]. "Free" picrates form hydrogen bonds with benzamide nitrogen [N(3)–H(3)···O(22)] and the coordinated oxygen of H_2O [O(7)–H(7A)···O(22)]. O(23) of "free" picrate forms a double-linked C–H···O hydrogen bond with phenyl C(4) [with H(4)] of neighboring molecules along

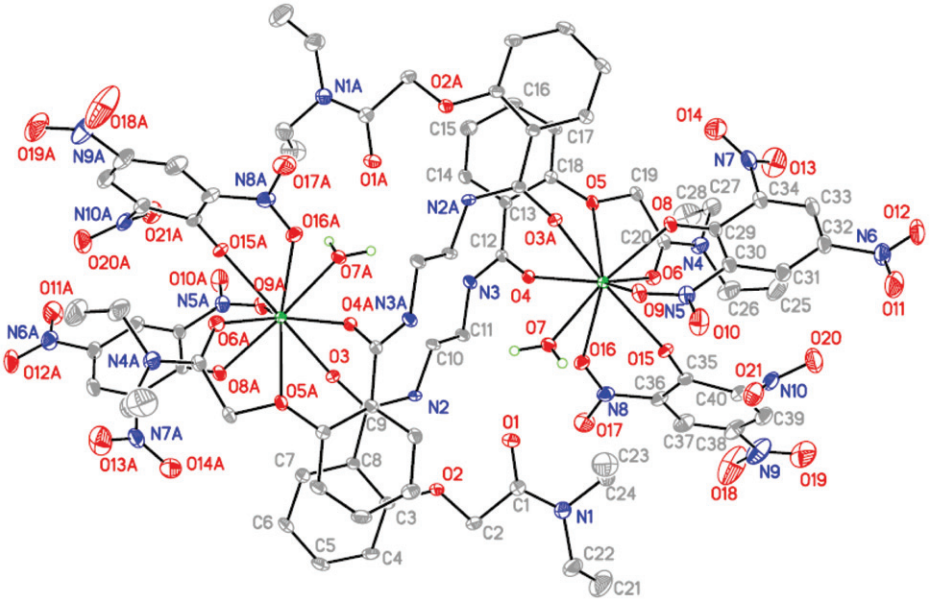

Figure 1. ORTEP diagram (20% probability ellipsoids) showing $[M_2L_2(Pic)_4(H_2O)_2]^{2+}$ of **3** (M = Eu), **6** (M = Dy), and **8** (M = Y).

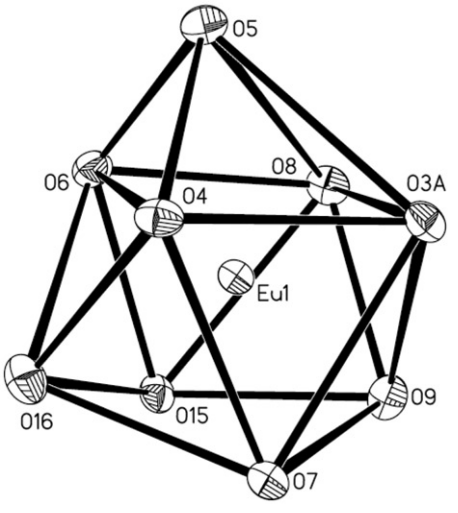

Figure 2. Coordination polyhedron of Eu1 ion.

the *a*-axis; C···O distances of 3.386(6) Å and the C–H···O angle θ of 150.7° indicate a strong interaction, leading to a 1-D chain. O(27) of the same "free" picrate forms another double-linked C–H···O hydrogen bond with phenyl C(16) [with H(16)] of another neighboring molecule; C···O distances of 3.354(6) Å and C–H···O angle θ of 140.9° form a 2-D sheet along the *ab*-plane by interweaving oxygen of free picrate with four neighboring molecules.

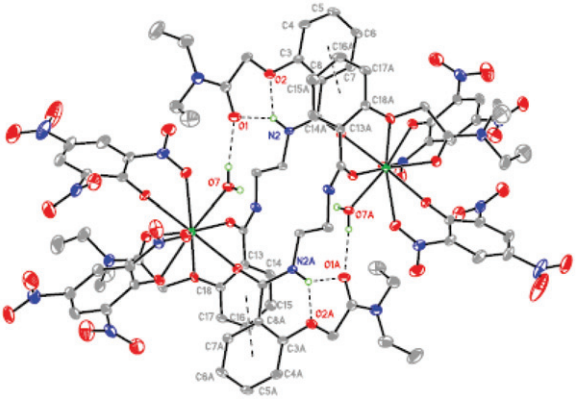

Figure 3. The intramolecular π–π interactions and hydrogen bonds (indicated by dashed lines) in $[M_2L_2(Pic)_4(H_2O)_2]^{2+}$.

Table 3. Hydrogen bonds for $[Eu_2L_2(Pic)_4(H_2O)_2](Pic)_2$ (Å, °).

D–H···A	*d*(D–H)	*d*(H···A)	*d*(D···A)	∠(D–H···A)
N(2)–H(2)···O(1)	0.86	2.45	3.126(5)	135.7
N(2)–H(2)···O(2)	0.86	1.88	2.576(5)	136.4
N(3)–H(3)···O(22)[a]	0.86	2.24	2.885(4)	131.6
O(7)–H(7A)···O(1)[b]	0.79	2.06	2.837(4)	172.4
O(7)–H(7B)···O(22)[a]	0.81	2.01	2.816(4)	178.8
C(4)–H(4)···O(23)′[c]	0.93	2.54	3.386(6)	150.8
C(16)–H(16)···O(27)′[d]	0.93	2.58	3.354(6)	140.9

Symmetry codes: [a] $1-x, 1-y, 1-z$; [b] $-x, 2-y, 1-z$; [c] $x, 1+y, z$; [d] $-2+x, y, z$.

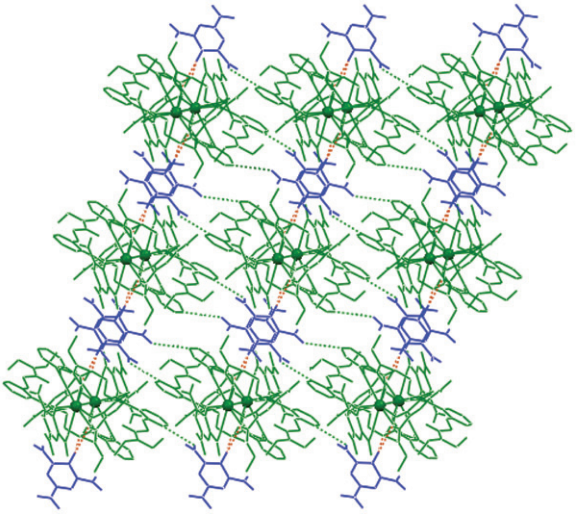

Figure 4. 2-D sheet generated by the intermolecular hydrogen bonds in **3** (the O(N)–H···O and C–H···O hydrogen bonds are indicated by dashed lines).

3.3. *IR spectra*

The complexes have similar IR spectra, suggesting that they have similar coordination. Characteristic absorptions of free ligand due to ν(Ar–C=O) are at 1659 cm^{-1}, ν(CH_2–C=O) at 1627 cm^{-1}, and ν(Ar–O–C) at 1248 cm^{-1}, respectively. After coordination, (Ar–)C=O bands of ligands shift to lower wavenumbers, (CH_2–)C=O bands become weak and new strong broader absorptions appear at 1614 cm^{-1}, indicating that oxygen atoms of all (Ar–)C=O bonds and part of (CH_2–)C=O bonds coordinate. Ar–O–C bands become weak and some ν(Ar–O–C) absorptions shift 25–29 cm^{-1} to lower wavenumbers, indicating that oxygen atoms of ether bonds of L take part in coordination. The band at 1265 cm^{-1} for ν(C–O) of Pic^- shifts to higher frequency by *ca* 7 cm^{-1} and the bands of free HPic due to ν_{as}(–NO_2) and ν_s(–NO_2) appear at 1555 and 1342 cm^{-1}, which split into two bands at *ca* 1574, 1542 cm^{-1} and *ca* 1361, 1330 cm^{-1}, respectively, in the complexes. These indicate that some oxygen atoms in the C–O bands and in the nitro groups of Pic^- participate in coordination [31]. Broad band at 3320 cm^{-1} indicates the presence of water, in agreement with the elemental analysis and crystal structure determination.

3.4. *Luminescent properties*

Among all eight complexes only the Eu(III) complex shows strong luminescent emission when excited in the solid state at room temperature and no ligand-based emission bands, indicating that the ligand is a good chelator to absorb and transfer energy to Eu ions (figure 5). The $^5D_0 \rightarrow {}^7F_2$ transition is much more intense than the $^5D_0 \rightarrow {}^7F_1$ transition; the intensity ratio $\eta(^5D_0 \rightarrow {}^7F_2/{}^5D_0 \rightarrow {}^7F_1)$ is 8.0, indicating that Eu^{3+} ions do not lie in a centro-symmetric coordination site [32], in agreement with the crystal structure analysis.

Based on the antenna effect, the intensity of the luminescence of lanthanide complexes is related to the efficiency of the intra-molecular energy transfer between the triplet levels of the ligand and the emitting level of lanthanide ions, which depends on the energy gap between the two levels. As all the complexes are isostructural, the energy of the ligand-centered triplet state does not depend significantly on the metal and the energy absorbed by the ligands could not be transferred to the lowest excited state of the

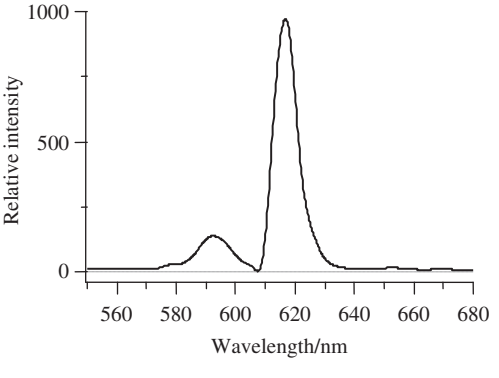

Figure 5. Emission spectra of the Eu complex in the solid state (excited at 420 nm).

Gd^{3+} ion (about 32,000 cm^{-1}). The phosphorescence spectrum of **4** $[Gd_2L_2(Pic)_4(H_2O)_2](Pic)_2$ was clearly observed at 77 K in a methanol–ethanol mixture (V : V = 1 : 1) to acquire the triplet excited state of L. The phosphorescence spectra demonstrated that the triplet energy levels (T1) of L and picrate are 23,810 cm^{-1} (420 nm) and 18,248 cm^{-1} (548 nm), respectively, both higher than the lowest excited resonance level $^5D_0$ of Eu(III) (17,300 cm^{-1}), confirming the suitability of the ligands as sensitizers for europium complexes [33]. The triplet state energy level T_1 of the ligand is also higher than the lowest excited resonance level $^5D_4$ of Tb(III) (20,500 cm^{-1}), but the luminescence of the Tb complex is not observed at room temperature. Energy is transferred from the triplet state of L to that of picrate and then transferred from the triplet state of picrate to the emitting level of rare-earth ions. The triplet state energy level of picrate (18,248 cm^{-1}, 548 nm) is lower than the lowest excited resonance level $^5D_4$ of Tb(III) (20,500 cm^{-1}). Therefore the intramolecular energy transfer between triplet levels of the ligand and the emitting level of terbium ions has been quenched by the picrate groups.

The influence of solvent on the luminescence intensities of the europium complex has also been studied. Luminescence spectra in ethyl acetate, tetrahydrofuran, dioxane, acetonitrile, acetone, methanol, and dimethylformamide solutions (concentration: 1.0×10^{-5} mol · cm^{-3}, the emission slit widths were 10 nm, figure 6) are recorded at room temperature. The fluorescence intensities of **3** in other solutions are lower than that in ethyl acetate and become weaker from THF, dioxane, MeCN, acetone, methanol to DMF due to the coordinating effects of solvents [34]. The rare-earth complexes have a dinuclear structure due to the balance between flexibility and rigidity of the amide-based acyclic polyether ligand and bulky picrate anions, but this structure could not prevent solvent from entering. Together with coordination abilities of THF, dioxane, MeCN, and DMF for lanthanides, the oscillatory motions of entering molecules induce non-radiative deactivation of the ligand triplet level transfer to the emitting level of the europium ion. Thus, the energy transfer could not be carried out perfectly. All of these indicate that solvents have strong coordination effect and the

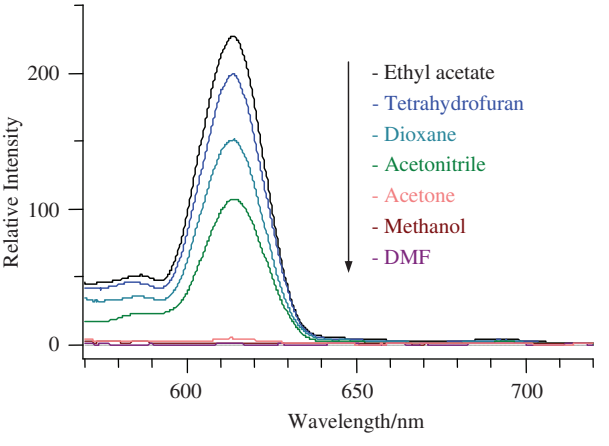

Figure 6. The emission spectrum of $[Eu_2L_2(Pic)_4(H_2O)_2](Pic)_2$ in ethyl acetate, THF, dioxane, MeCN, acetone, methanol, and DMF solutions at room temperature. Concentration: 1.0×10^{-5} mol · cm^{-3}.

environment plays an important role in determining the fluorescence intensity of the complexes [17, 35].

4. Conclusion

New dinuclear rare-earth picrate complexes, $[M_2L_2(Pic)_4(H_2O)_2](Pic)_2$, where $M = La^{3+}$ (**1**), Nd^{3+} (**2**), Eu^{3+} (**3**), Gd^{3+} (**4**), Tb^{3+} (**5**), Dy^{3+} (**6**), Yb^{3+} (**7**), Y^{3+} (**8**), have been prepared and characterized. The amide-based acyclic polyether forms stable complexes with rare-earth picrates and IR spectral changes were observed after coordination. X-ray structure analyses show that the dinuclear complexes are isomorphous and each has one coordination cation and two free picrates as the counter anions. With hydrogen bonds between them the complexes exhibit a 2-D net supermolecule. The Eu(III) complex shows strong luminescence emission in the solid state at room temperature, indicating that the ligand is a good chelator to sensitize Eu(III) emission. The influence of solvent on the fluorescence intensities indicates that solvent and environment play important roles in determining the fluorescence intensity of the complexes.

Supplementary material

CCDC 600837, 610281, and 610284 contain the supplementary crystallographic data for **3**·$2C_4H_8O_2$, **6**·$2C_4H_8O_2$, and **8**·$2CH_3CN$, respectively. These data can be obtained free of charge from the Cambridge Crystallographic Data Centre *via* www.ccdc.cam.ac.uk/data_request/cif. Supplementary material associated with this article can be found in supporting information section.

Acknowledgments

The work was supported by the Fundamental Research Funds for the Central Universities (lzujbky-2011-114), the National Natural Science Foundation of China for Personnel Training (J1103307), and the National Natural Science Foundation of China (21171077, 51074083).

References

[1] L.-Y. Zhu, X.-F. Tong, M.-Z. Li, E.-J. Wang. *J. Phys. Chem. B*, **105**, 2461 (2001).
[2] J. Kido, Y. Okamato. *Chem. Rev.*, **102**, 2357 (2002).
[3] J.-C.G. Bünzli, C. Piguet. *Chem. Soc. Rev.*, **34**, 1048 (2005).
[4] J.-C.G. Bünzli, A.-S. Chauvin, H.K. Kim, E. Deiters, S.V. Eliseeva. *Coord. Chem. Rev.*, **254**, 2623 (2010).
[5] T. Jüstel, H. Nikol, C. Ronda. *Angew. Chem. Int. Ed.*, **37**, 3084 (1998).
[6] N. Sabbatini, M. Guardigli, J.-M. Lehn. *Coord. Chem. Rev.*, **123**, 201 (1993).
[7] M. Elhabiri, R. Scopelliti, J.-C.G. Bünzli, C. Piguet. *J. Am. Chem. Soc.*, **121**, 10747 (1999).

[8] R.S. Dickins, J.A.K. Howard, C.W. Lehmann, J. Moloney, D. Parker, R.D. Peacock. *Angew. Chem. Int. Ed. Engl.*, **36**, 521 (1997).
[9] B. Alpha, R. Ballardini, V. Balzani, J.-M. Lehn, S. Perathoner, N. Sabbatini. *Photochem. Photobiol.*, **52**, 299 (1990).
[10] P.L. Jones, A.J. Amoroso, J.C. Jeffery, J.A. Mccleverty, E. Psillakis, L.H. Ress, M.D. Ward. *Inorg. Chem.*, **36**, 10 (1997).
[11] S.-S. Xiao, X.-J. Zheng, S.-H. Yan, X.-B. Deng, L.-P. Jin. *CrystEngComm*, **12**, 3145 (2010).
[12] W.-T. Chen, Z.-L. Yao. *J. Coord. Chem.*, **64**, 996 (2011).
[13] D.-J. Qian, W.-N. Zhang, Z. Chen, J.V. Houten. *Spectrochim. Acta, Part A*, **56**, 2645 (2000).
[14] F.-H. Liu, Y.-B. Zhou. *Inorg. Chem. Commun.*, **13**, 1410 (2010).
[15] W.P.-W. Lai, W.-T. Wong, B.K.-F. Li, K.-W. Cheah. *New J. Chem.*, **26**, 576 (2002).
[16] K.R. Adam, I.M. Atkinson, J. Kim, L.F. Lindoy, O.A. Matthews, G.V. Meehan, F. Raciti, B.W. Skelton, N. Svenstrup, A.H. White. *J. Chem. Soc., Dalton Trans.*, 2388 (2001).
[17] W. Wang, Y. Huang, N. Tang. *Spectrochim. Acta, Part A*, **66**, 1058 (2007).
[18] W.-N. Wu, F.-X. Cheng, L. Yan, N. Tang. *J. Coord. Chem.*, **61**, 2207 (2008).
[19] K. Nakagawa, K. Amita, H. Mizuno, Y. Inoue, T. Hakushi. *Bull. Chem. Soc. Japan*, **60**, 2037 (1987).
[20] J.B. Gandhi, N.D. Kulkarni. *J. Chem. Res. (S)*, **12**, 488 (1994).
[21] J. Speziale, P.C. Hamm. *J. Am. Chem. Soc.*, **78**, 2556 (1956).
[22] SAINT. *Software Reference Manual*, Bruker AXS, Madison, WI (1998).
[23] G.M. Sheldrick. *SHELXTL NT Version 5.1*, *Program for Solution and Refinement of Crystal Structures*, University of Göttingen, Germany (1997).
[24] W.J. Geary. *Coord. Chem. Rev.*, **7**, 81 (1971).
[25] K.-W. Lei, W.-L. Liu, M.-Y. Tan. *Spectrochim. Acta, Part A*, **66**, 118 (2007).
[26] T.L. Borgne, J.-M. Bénech, S. Floquet, G. Bernardinell, C. Aliprandini, P. Bettens, C. Piguet. *Dalton Trans.*, 3856 (2003).
[27] G. Bernardinelli, C. Piguet, A.F. Williams. *Angew. Chem. Int. Ed.*, **12**, 1622 (1992).
[28] C. Piguet, J.-C.G. Bünzli, G. Bernardinelli, G. Hopfgartner, A.F. Williams. *J. Am. Chem. Soc.*, **115**, 8197 (1993).
[29] G.R. Desiraju. *Acc. Chem. Res.*, **29**, 441 (1996).
[30] T. Steiner. *Angew. Chem. Int. Ed.*, **41**, 48 (2002).
[31] S.-X. Liu, W.-S. Liu, M.-T. Tan, K.-B. Yu. *J. Coord. Chem.*, **10**, 391 (1996).
[32] A.F. Kirby, D. Foster, F.S. Richardson. *Chem. Phys. Lett.*, **95**, 507 (1983).
[33] P. He, H.-H. Wang, S.-G. Liu, J.-X. Shi, G. Wang, M.-L. Gong. *Inorg. Chem.*, **48**, 11382 (2009).
[34] H.Q. Liu, T.C. Cheung, C.M. Che. *Chem. Commun.*, 1039 (1996).
[35] D.-J. Zhou, Q. Li, C.-H. Huang, G.-Q. Yao, S. Umetani, M. Matsui, L.-M. Ying, A.-C. Yu, X.-S. Zhao. *Polyhedron*, **16**, 1381 (1997).